



Cite this: *Phys. Chem. Chem. Phys.*, 2016, 18, 18024

Metal ion–humic acid nanoparticle interactions: role of both complexation and condensation mechanisms†

Raewyn M. Town*^a and Herman P. van Leeuwen^b

Purely Donnan type models for electrostatic binding by humic acid (HA) nanoparticles are shown to be physically incomplete. To describe the extent of ion binding by HA, such models need to invoke parameters that are not consistent with experimental observations. These disparate parameters include anomalously high Donnan potentials, as well as intrinsic affinity constants for electrostatically associating ions such as Ca^{2+} . In contrast, the recently introduced counterion condensation – Donnan model (CCD) provides a physicochemically realistic description of the electrostatic contribution to metal ion binding by humic acid nanoparticles. The extent of Ca^{2+} –HA association can be adequately described solely in terms of electrostatics only, including counterion condensation in the intraparticle double layer in addition to Donnan partitioning in the remainder of the particle body. The binding of $\text{Cd}(\text{II})$, $\text{Pb}(\text{II})$ and $\text{Cu}(\text{II})$ by HA also involves inner-sphere complex formation leading to intraparticle metal species distributions with major proportions of condensed and complexed ions.

Received 20th April 2016,
Accepted 13th June 2016

DOI: 10.1039/c6cp02634f

www.rsc.org/pccp

1 Introduction

Humic acids (HA) are ubiquitous in soils and natural waters and form an important complexant for a wide range of ions and small molecules.¹ Accordingly, there is a wealth of literature on the measurement and modelling of its physicochemical association properties.^{1–3} Aqueous HA can be considered to be composed of soft nanoparticles (NP) that carry a net negative charge at ambient pH.^{4,5} Indeed, the large number of ionisable functional groups generate a significant particle electric field, which in itself can influence the dynamics and extent of its interactions with oppositely charged ions, M^{z+} .⁶ Rigorous interpretation of physicochemical M–HA interactions must therefore take proper account of electrostatic interactions as well as intrinsic chemical contributions to the binding.

Conventionally, M–HA complex formation is described in terms of apparent stability constants, \bar{K}_{app} , that are defined in terms of concentrations of chemical species that are averaged over the entire volume of the solution/dispersion. Furthermore, so-called ‘bound’ M is collectively taken as all forms of M that are associated with the HA entity, including intraparticle

free M and even the excess free M in the extraparticle interfacial double layer. At this level, various equilibrium models for metal ion speciation have been developed, e.g. the NICA–Donnan² and WHAM³ models. Generally the electrostatic contribution to M^{z+} binding by HA is modeled by assuming Donnan-type partitioning into the HA body or Boltzmann-type accumulation in the extraparticle zone.^{3,7–12} The relevant physicochemical parameters then are the effective Donnan volume and the charge density of the HA particle. The various affinities of the functional M^{z+} binding sites are modeled either by a number of different types of discrete sites, e.g. WHAM,³ or by a continuous distribution of site affinities, e.g. NICA–Donnan.² Evidently the meaning of \bar{K}_{app} values is not transparent for the case of nanoparticle complexants in which binding sites are confined to the particle body within which the local conditions are significantly different from those in the bulk aqueous medium. For example, \bar{K}_{app} values increase as the ionic strength of the bulk aqueous medium decreases.^{13,14} This observation is not due to a significant change in the intrinsic chemical affinity, but rather is a consequence of the greater free M concentration within the HA entity at lower ionic strength. Obviously, a more rigorous description of M–HA complex formation requires detailed knowledge of both electrostatic and intrinsic chemical affinity contributions to the binding and the ensuing consequences for the detailed metal ion speciation inside the HA particle entity.

Recently the nature of electrostatic binding by HA has been reconsidered.¹⁵ The typically high structural charge densities,

^a Department of Physics, Chemistry and Pharmacy, University of Southern Denmark, Campusvej 55, 5230 Odense, Denmark. E-mail: raewyn.town@sdu.dk

^b Physical Chemistry and Soft Matter, Wageningen University & Research, Stippeneng 4, 6708 WE Wageningen, The Netherlands

† Electronic supplementary information (ESI) available. See DOI: 10.1039/c6cp02634f



that prevail within the particle body at ambient pH, invoke cooperative electrostatics effects such as counterion condensation, which features a large preference for the higher valency cations. Such phenomena have been described in detail by Manning for linear polyelectrolytes,^{16,17} and refer to the tendency of the polyion to condense counterions in its immediate vicinity if the structural charge density is beyond certain limiting values. Counterion condensation is applicable to polyions of any geometry with sufficient charge density, *e.g.* it has been reported for polyelectrolytes such as DNA,¹⁶ soft nanoparticles such as dendrimers,^{18–20} as well as core–shell NPs with a 3D structural charge in the shell.²¹ We have observed that counterion condensation in the 3D site distribution structure occurs at charge separations greater than for the 1D case.¹⁵ For HA, conductivity data have shown that divalent ions such as Ca²⁺ and Ba²⁺ exhibit condensation behavior, whilst monovalent ions do not.²² Notably, it was shown that the extent of electrostatic association of Ca²⁺ with HA cannot be explained by Donnan-partitioning alone. The CCD model therefore combines counterion condensation in the intraparticulate double layer with Donnan partitioning in the remainder of the particle body. It well describes the extent to which Ca²⁺ associates with a range of HA samples with different particle sizes at various ionic strengths.¹⁵ It has also been applied to the intraparticulate speciation analysis of complexes that involve covalency, *i.e.* those of Cd(II), Pb(II), and Cu(II).²³ Three types of intraparticulate metal species then are distinguished, namely free hydrated ions, electrostatically condensed ions, and inner-sphere complexes. Here we compare the CCD description of M–HA interactions with the results generated by equilibrium speciation models that consider Donnan-type partitioning to be the only electrostatic contribution to the binding. We explore the nature of the fundamental parameters that are relevant for defining the extent of complexation, *e.g.* the effective Donnan volume and the applicable charge density, and assess the outcomes in terms of the physical consistency.

2 Theory

The equilibrium relationship between the concentrations of the metal ion and the various binding sites of the chemically heterogeneous HA complexant is described by a distributed affinity. The apparent stability constants \bar{K}_{app} for the complexes are expressed in terms of smeared-out concentrations and include both electrostatic and intrinsic chemical contributions to the binding between a metal ion M and a reactive site, S. The magnitude of \bar{K}_{app} depends on the degree of occupation, θ_{M} , of the binding sites by M.¹ We define θ_{M} as the ratio between the concentrations of inner-sphere metal complexes, MS, and reactive sites, *i.e.*

$$\theta_{\text{M}} = c_{\text{MS}}/c_{\text{S,t}} = c_{\text{MS}}^*/c_{\text{S,t}}^* \quad (1)$$

where c_{MS} and $c_{\text{S,t}}$ are the local intraparticulate concentrations of the inner-sphere complexes and total reactive sites, respectively, and c_{MS}^* and $c_{\text{S,t}}^*$ are the smeared-out counterparts.

2.1 Intrinsic stability constants

The intrinsic stability constant K_{int} represents the inherent chemical affinity between M and S, not including the long-range electrostatics beyond those on the scale of atom–atom interactions. K_{int} values may only be obtained from K_{app} after applying the appropriate correction for the electrostatic contribution to the binding. For simple ligands, the outer-sphere stability constant, K^{os} , represents the magnitude of the electrostatic attraction between a negatively charged reactive site and a positively charged metal ion. The extent to which the concentration of the reactant metal ions in the outer-sphere volume is enhanced relative to that in the bulk electrolyte medium, f^{os} , can be computed on the basis of Fuoss–Boltzmann electrostatics.^{24,25}

$$f^{\text{os}} = \exp(-U^{\text{os}}/kT) \quad (2)$$

where U^{os} is the interionic potential for an individual ion pair, given by:

$$U^{\text{os}} = \frac{z_{\text{M}}z_{\text{S}}e^2}{4\pi\epsilon_0\epsilon a} \left(1 - \frac{\kappa a}{1 + \kappa a}\right) \quad (3)$$

where a is the center-to-center distance between M and S, z_{M} and z_{S} are the charge on the metal ion and the binding site, respectively, and $\epsilon_0\epsilon$ is the permittivity of the electrolyte solution. It follows that for simple ligands:

$$K_{\text{int}} = K/f^{\text{os}} \quad (4)$$

where K is the conventional stability constant for a simple ligand. *E.g.* for a 2+/1– ion pair with a center-to-center distance of 0.6 nm, the values of f^{os} are approximately 4 and 7 for ionic strengths of 100 and 10 mol m^{−3}, respectively.

For the case of soft charged nanoparticulate complexants, the magnitude of the particle's electric field determines the extent to which oppositely charged ions electrostatically associate with the NP entity. The majority of literature for humic acids assumes that this association takes the form of Donnan partitioning into the NP body. The establishment of a Donnan phase requires that the particle radius is much greater than the intraparticulate screening length, κ_{p}^{-1} ,³³ and that the average structural charge separation, ℓ_{C} , is sufficiently small so that $\kappa_{\text{p}}\ell_{\text{C}} \ll 1$, *i.e.* high charge density regime.⁵ When these conditions are met, a Donnan potential difference, ψ_{D} , is established between the bulk of the soft phase and the bulk aqueous medium:²⁶

$$\psi_{\text{D}} = \frac{RT}{zF} \text{asinh}\left(\frac{\rho_{\text{p}}}{2zFc_1}\right) \quad (5)$$

where $z_- = z_+ = z$ is the valency of the symmetrical excess background electrolyte with bulk concentration c_1 , ρ_{p} is the structural volume charge density due to charged groups on the backbone of the soft body, and other constants have their usual meaning. Expressions are also available for asymmetrical electrolytes.²⁶ Any type of ion i , with valency z_i , will partition between the soft particle phase (where its concentration is $c_{i,\text{D}}$) and the electrolyte solution (where its concentration is c_i^*) according to a Boltzmann factor, $\bar{f}_{\text{B},i}$:²⁷

$$\bar{f}_{\text{B},i} = \frac{c_{i,\text{D}}}{c_i^*} = \exp\left(\frac{-z_i F \psi_{\text{D}}}{RT}\right) \quad (6)$$



When Donnan partitioning is the sole electrostatic contribution to the binding of M by S, the \bar{K}_{int} is simply given by:

$$\bar{K}_{\text{int}} = \bar{K}_{\text{app}}/\bar{f}_B \quad (7)$$

However, recent work has provided evidence for additional electrostatic binding due to counterion condensation. A two-state approximative model was developed which combines Donnan partitioning within the uncharged bulk zone of the soft NP (volume V_D and volume fraction φ_D) with counterion condensation in the strongly negatively charged intraparticulate double layer zone of thickness ℓ_{DL} (with volume V_{DL} and volume fraction φ_{DL}).^{15,23} The justification of a constant Donnan potential throughout the bulk core volume of the particle requires a volume fraction ratio $\varphi_{\text{DL}}/\varphi_D$ much less than unity, *i.e.* $\kappa_p r_p$ should be well above unity. In this work we focus on HA entities for which $\varphi_{\text{DL}}/\varphi_D$ is less than 0.1. In the presence of counterion condensation, the distinction between \bar{K}_{app} and \bar{K}_{int} encompasses more than the Boltzmann correction of the free metal ion (*cf.* eqn (7)). Rather, the intrinsic stability constant is defined in terms of intraparticulate (*in situ*) conditions and reactant concentrations, *i.e.*

$$\bar{K}_{\text{int}} = \frac{c_{\text{MS}}}{c_{\text{S}}c_{\text{M},f}} \quad (8)$$

where c_{MS} , $c_{\text{M},f}$ and c_{S} are the local average concentrations of inner-sphere complexes, free metal ion and reactive sites in the particle body, respectively, and the bar in \bar{K}_{int} signifies that, for the present case of a heterogeneous complexant, the intrinsic stability represents a weighted average of all the inner-sphere complexes that are formed at the applicable θ_{M} . The ensuing metal ion speciation scheme for high charge density soft NP complexants has been published previously,²³ and is given in the ESI† (Table S1). We highlight that our approach makes no assumptions about the nature of the charged or reactive sites, nor about the metal binding isotherm.

3 Experimental

The experimental details for the data presented herein were reported previously.²³ NICA-Donnan computations were performed using Visual Minteq 3.1 and the generic HA parameters.²⁸ The local concentrations were determined from the smeared-out concentrations that were fitted by the model in each computation, together with the generic Donnan volume. For each type of complexing ion, NICA-Donnan assumes a bimodal affinity distribution: for the present comparative purposes, the sum of the complexes with both types of sites was used to compute the proportion of inner-sphere complexes.

4 Results and discussion

4.1 Electrostatic contribution to the binding

The physical size of the HA nanoparticle in aqueous dispersion is important for both the Donnan-only and the two-state CCD electrostatic models. A water content of *ca.* 80% has been reported for several types of HA from viscometric data at pH 7 and ionic strengths of 10 and 100 mol m⁻³.²⁹ For establishment

of the CCD approach, the water content of about 80% provided a consistent description of the Ca²⁺ association with several types of HA, including Aldrich HA, at ionic strengths of 10 and 100 mol m⁻³ [see ref. 15 and references therein]. This consistent water content at both ionic strengths is in line with experimental estimates of the particle size of various types of HA by dynamic light scattering, capillary electrophoresis, and fluorescence correlation spectroscopy which confirm that the HA particle size is practically independent of ionic strength in the range 0 to 200 mM.^{30–32} Due to the presence of a large density of structural charged sites with insignificant local mobility, there is uncertainty about the magnitude of the effective intraparticulate Debye length κ_p^{-1} . Duval³³ has made some estimations of this crucial parameter which come to approximately 0.6 nm for both 10 and 100 mol m⁻³ ionic strength in the surrounding medium. The binding of Ca²⁺ by the HA studied here has been interpreted in terms of a thickness of the electric condensation zone, ℓ_{DL} , for which the magnitude was obtained from fitting to agreement with the potential change over the intraparticulate part of the interfacial double layer.¹⁵ There should be a close relationship between ℓ_{DL} and κ_p but to our knowledge this has not yet been formulated. For the time being we can proceed by accepting the magnitude of ℓ_{DL} together with the degree of Ca²⁺ condensation as the leading numbers for the condensation of any other divalent metal ion. See Section 4.2 below for details. Accordingly, within the total particle volume, V_p , the CCD model distinguishes between an intraparticulate double layer shell with volume V_{DL} , and a Donnan phase with volume $V_D = V_p - V_{\text{DL}}$. For the present system with $\kappa_p r_p \gg 1$ and both ionic strengths investigated, V_D is close to the total particle volume.

The Donnan volume used in the NICA-Donnan model is obtained by fitting a combination of V_D and ψ_D to a so-called mastercurve for protolytic titrations of HA.⁷ An empirical double logarithmic expression links the Donnan volume to the ionic strength of the bulk medium:¹²

$$\log V_D = b(1 - \log I) - 1 \quad (9)$$

where b is a fitting parameter and I the ionic strength of the medium. Thus eqn (9) indicates that V_D is significantly dependent on I , even though V_p is practically independent of I (see above). Apart from this discrepancy, the physical reasonableness of the NICA-Donnan V_D and ψ_D values has been questioned on the basis that the generic values for ψ_D are significantly more negative than those experimentally determined for HA, and the concomitantly fitted protonation constants are anomalously low.^{34,35} It should also be noted that the approach used to obtain the NICA-Donnan V_D , ψ_D couple involves covariance of several parameters and the outcome is sensitive to how the fitting is implemented. For example, a modified procedure that minimizes the covariance of the NICA-Donnan parameters and optimizes the b value for each ionic strength, yields protonation constants that are in better agreement with literature data, in combination with a different b .³⁴

In passing we note that the WHAM speciation model assumes Donnan partitioning to occur only within the extraparticulate double layer, irrespective of the particle size.³ The occurrence of



extraparticulate “Donnan partitioning” is also allowed in the NICA-Donnan model for fulvic acids and small humic acids for which the fitted Donnan volume is allowed to be greater than the particle size.³⁶ However, the extraparticulate double layer carries a net charge density and does not contain any fixed charges at all, *i.e.* it is not a true Donnan phase. Rather, Boltzmann accumulation should be expected to occur in such zones. For $\kappa_p r_p$ of order unity and lower, the amount of M^{2+} in the extraparticulate DL may indeed be significant in the total amount of M associated with the particle. In the CCD, the excess amount of M in the extraparticulate DL is straightforwardly obtained from the Boltzmann accumulation of M^{2+} as ensuing from the diffuse double layer potential profile³⁷ and included in the mass balance for particle-associated free M .

The approaches for modeling the electrostatic contribution to cation binding by HA are summarized in Table 1 below.

The equilibrium speciation in a range of M -HA systems has been modeled by the NICA-Donnan approach, with typically good fits to the experimentally measured free metal ion concentrations being reported.³⁸ Despite their very different constituent parameters, the WHAM and NICA-Donnan models predict similar concentrations of free metal ions in the presence of dissolved organic matter.³⁹ This observation points to the empirical nature of the models. The quality-of-fit of the models is assessed on the basis of agreement between the measured and computed ‘free’ *versus* ‘bound’ M , where ‘bound’ includes all forms of M associated with the HA entities. However, the physical meaning of the various parameters in these equilibrium models is obscured due to the concomitant nature of the fitting process, and the interrelationships between the sub-models for intrinsic chemical and electrostatic binding components.²⁸ Indeed, a recent review of the NICA-Donnan approach stated “The fact that a set of parameter values can be non-unique is first of all due to the large number of parameters in the model. A different way of fitting of the parameters to the data may lead to an equally good description of the data, but different parameter values.”²

4.2 Speciation in the electrostatic Ca^{2+} -HA system

Here we seek to identify the physicochemically most reasonable descriptors for the binding of M^{2+} by HA. As a straightforward starting point, we consider the case of Ca^{2+} association with HA. The associative reactions of Ca^{2+} with negatively charged functional groups are dominated by electrostatics.^{40–42} The extent to which Ca^{2+} associates with HA was found to be far greater than that predicted by only Donnan-type electrostatics,

with more highly charged HAs exhibiting the greatest amount of Ca^{2+} association.¹⁵ Accordingly, in order to describe the Ca^{2+} -HA data, the NICA-Donnan model resorts to inclusion of intrinsic affinity constants for Ca^{2+} complexation, together with V_D values that are smaller for more highly charged humic acids. For example, the NICA-Donnan V_D values fitted to Ca^{2+} -HA binding data follow the inverse order of the HA charge density: *e.g.* for Elliot soil HA with carboxyl content 4.8 mol kg^{-1} , V_D is $0.23 \times 10^{-3} \text{ m}^3 \text{ kg}^{-1}$, with a concomitant protonation constant ($K_{1,H}$) of $10^{-0.8} \text{ m}^3 \text{ mol}^{-1}$ significantly lower than the generic value of $10^{-0.1} \text{ mol m}^{-3}$,⁴³ whilst for a forest soil HA with carboxyl content 2.18 mol kg^{-1} , V_D is $2.95 \times 10^{-3} \text{ m}^3 \text{ kg}^{-1}$, using the generic protonation constants.⁴⁴ An example of the speciation computed by the NICA-Donnan model for the Ca^{2+} -HA system is given in Table 2. The fit to the data invokes a ψ_D of *ca.* -100 mV , which is rather negative for the given ionic strength of 82 mol m^{-3} ,⁴⁵ as well as inner-sphere Ca^{2+} complex formation. As much as 81% of the particle-associated Ca^{2+} is predicted to be inner-sphere bound, whereas the K_{int} for CaHA is similar to its purely electrostatic K^{os} which would hardly suggest any inner-sphere complexes at all.

In contrast, the CCD model describes the extent of Ca^{2+} -HA association for a range of HA samples, pH and ionic strength values, *via* inclusion of the mere electrostatic contributions due to counterion condensation within the intraparticulate double layer, together with a more realistic ψ_D of -70 mV in the bulk of the particle body (Table 2).

4.3 Intraparticulate speciation with inner-sphere complexes M-HA

Here we consider the speciation in M -HA systems in which intrinsic chemical binding is also involved, and compare the results obtained by the CCD and NICA-Donnan approaches. The parameters defining the CCD speciation scheme are given in the ESI.† Table 3 collates the concentrations of the various metal species for the case of a 1-1 background electrolyte (KNO_3). In the CCD case, the given intraparticulate \bar{K}_{int} values are those derived from local concentrations after accounting for the electrostatic effects (eqn (8)), whilst the NICA-Donnan values are obtained *via* eqn (7).

The data show that for both approaches the free hydrated metal ions generally are a minor proportion of the total intraparticulate M . The CCD results for Cd(II) at $I = 100 \text{ mol m}^{-3}$, show that 70% of the uncomplexed M is condensed in the intraparticulate double layer and 30% is inner-sphere bound,

Table 1 Models for electrostatic binding by humic acid

Model	Electrostatic binding	Donnan volume, V_D , relative to particle volume, V_p
WHAM ³	Donnan partitioning ^a	V_D entirely extraparticulate $V_D = \frac{4\pi N_{Av}}{3} [(r_p + \kappa^{-1})^3 - r_p^3]$
NICA-Donnan ²	Donnan partitioning ^a	V_D may be smaller or larger than the physical V_p . $\log V_D = b(1 - \log I) - 1$, where b is an empirical factor with generic value of 0.49 for HA
CCD ²³	Counterion condensation plus Donnan partitioning ^b	$V_D = V_p - V_{DL}$

^a Irrespective of the physical particle size. ^b For $\kappa_p r_p \gg 1$, in high charge density regime.



Table 2 Speciation computed in the Ca^{2+} –HA system by CCD and NICA-Donnan approaches. $c_{\text{Ca,t}}^* = 0.195 \text{ mol m}^{-3}$, $c_{\text{HA,t}}^* = 2000 \text{ g m}^{-3}$, $\text{pH} = 8$ and $I = 82 \text{ mol m}^{-3}$ in bulk electrolyte medium^a

	CCD ^b	NICA-Donnan ^c
$c_{\text{Ca,f}}^*$, mol m^{-3}	3.8×10^{-3}	7.8×10^{-3}
$c_{\text{Ca,t}}^*$, mol m^{-3}	38	88.5
Fraction free in V_{DL}	4×10^{-3}	—
Fraction free in V_{D}	0.03	0.19
Fraction condensed in V_{DL}	0.97	—
Fraction inner-sphere MS	—	0.81
$\bar{f}_{\text{B,M}}$ in V_{D}	250	2130

^a Experimental data from Hering and Morel.⁴⁶ ^b Computed using the experimentally measured concentration of free Ca^{2+} in the bulk medium, together with a condensation factor, \bar{f}_{C} , of 0.8 in the intraparticulate double layer with thickness of 2 nm,²³ and a volume charge density of $-1300 \text{ mol e m}^{-3}$ at $\text{pH} 8$.⁴⁷ ^c Computed using the NICA-Donnan generic parameters²⁸ for the given total concentrations of Ca^{2+} and HA.

whilst Pb(II) and Cu(II) are approximately equally distributed between these two forms. Furthermore, the total concentration of Cd(II) , Pb(II) and Cu(II) associated with the particles is similar at $I = 100$ and 10 mol m^{-3} . In contrast, in practically all cases considered the NICA-Donnan model predicts that the vast majority of the intraparticulate M is in the form of inner-sphere complexes (Table 3). It also predicts a much greater total concentration in the particle body at an ionic strength of 100 mol m^{-3} as compared to 10 mol m^{-3} . This outcome is a consequence of the ionic strength dependence of the NICA-Donnan V_{D} value which translates to, for equivalent total mass in the dispersion, the volume fraction of HA being a factor of 6 times lower at an ionic strength of 100 mol m^{-3} as compared to 10 mol m^{-3} , in contradiction with experimental findings (see Section 4.1).

The extent to which Ca^{2+} electrostatically associates with HA provides a useful means to probe the consistency of the speciation results for Cd^{2+} , Pb^{2+} and Cu^{2+} given in Table 3. That is, the deliberate use of a calcium salt, *e.g.* $\text{Ca}(\text{NO}_3)_2$, as the background electrolyte, with a concentration of Ca^{2+} several orders of magnitude greater than that of the target M^{2+} , enables

the electrostatic contribution to the binding of M^{2+} to be eliminated. This feature is a consequence of the purely electrostatic counterion condensation demands of the HA entity being practically totally met by the abundant Ca^{2+} . Accordingly, in terms of the CCD approach the intraparticulate speciation of M^{2+} will involve only Donnan-type partitioning in V_{D} , Boltzmann accumulation in V_{DL} and inner-sphere complexation in V_{D} and V_{DL} . It should be noted that for a given ionic strength, the effective Donnan potential in the 2:1 electrolyte is lower than in the standard 1:1 electrolyte (*cf.* eqn (5)). For comparison, computations were performed with the NICA-Donnan model in $\text{Ca}(\text{NO}_3)_2$ media for the same bulk concentrations of HA and M(II) as used in the experiments reported herein.

Several factors must be taken into account in comparing the \bar{K}_{int} values derived for the different ionic strengths in KNO_3 *vs.* $\text{Ca}(\text{NO}_3)_2$ electrolyte. As described above, in $\text{Ca}(\text{NO}_3)_2$ there is no counterion condensation of the target M^{2+} and the Donnan potential is lower than that in KNO_3 . Accordingly, the intraparticulate environments in KNO_3 *vs.* $\text{Ca}(\text{NO}_3)_2$ electrolyte differ in terms of the net charge density and the corresponding ψ_{D} , the ensuing magnitude of $\bar{f}_{\text{B,M}}$ for the intraparticulate free M^{2+} , and the effective charge screening. In comparing the behavior of Cd(II) , Pb(II) and Cu(II) , we must also take into account the different chemical affinities of these transition metal ions for the reactive sites as well as the heterogeneous nature of the HA complexant. The chemical affinity of the target M^{2+} towards the major complexing groups of HA follows the order $\text{Cd(II)} < \text{Pb(II)} \approx \text{Cu(II)}$, whilst their degree of heterogeneity follows $\text{Cd(II)} < \text{Pb(II)} < \text{Cu(II)}$.¹ The overall consequence for each M^{2+} is that \bar{K}_{int} decreases as θ_{M} increases, with the magnitude of this effect being governed by the heterogeneity of the complexes. That is, for a given increase in θ_{M} , the \bar{K}_{int} for Cu(II) is expected to decrease by a greater extent than that for Cd(II) .

With the above features in mind, we consider the physico-chemical reasonableness of the CCD and NICA-Donnan results. The case of Cd(II) at $I = 100 \text{ mol m}^{-3}$ provides a strong test of the consistency of the two approaches: at the metal-to-site ratio considered, inner-sphere binding is rather weak, and both

Table 3 Comparison of intraparticulate speciation obtained *via* the CCD and NICA-Donnan (NICAD) models for KNO_3 electrolyte. $c_{\text{M,t}}^* = 4.6 \times 10^{-3} \text{ mol m}^{-3}$; $c_{\text{HA,t}}^* = 50 \text{ g m}^{-3}$; $\text{pH} = 6$ in bulk electrolyte medium

	Cd , $I = 100 \text{ mol m}^{-3}$		Cd , $I = 10 \text{ mol m}^{-3}$		Pb , $I = 100 \text{ mol m}^{-3}$		Pb , $I = 10 \text{ mol m}^{-3}$		Cu , $I = 100 \text{ mol m}^{-3}$		Cu , $I = 10 \text{ mol m}^{-3}$	
	CCD	NICAD	CCD	NICAD	CCD	NICAD	CCD	NICAD	CCD	NICAD	CCD	NICAD
$c_{\text{M,f}}^*$, mol m^{-3}	1×10^{-3}	1.8×10^{-3}	3×10^{-4}	5.7×10^{-4}	3×10^{-7}	4.1×10^{-5}	6.5×10^{-8}	9.5×10^{-6}	7×10^{-7}	3.6×10^{-6}	4×10^{-7}	9.1×10^{-7}
$c_{\text{M,t}}^*$, mol m^{-3}	28.6	54.4	34.1	27.2	36.5	95.0	36.5	31.1	36.5	96.2	36.5	31.2
Fraction free in V_{DL}	3×10^{-5}	—	2×10^{-4}	—	8×10^{-9}	—	3.5×10^{-8}	—	2×10^{-8}	—	2×10^{-7}	—
Fraction free in V_{D}	2×10^{-3}	0.03	0.04	0.16	4×10^{-7}	4×10^{-4}	8×10^{-6}	2.4×10^{-3}	9×10^{-7}	3.5×10^{-5}	5×10^{-5}	2.3×10^{-4}
Fraction condensed in V_{DL}	0.7	—	0.55	—	0.5	—	0.5	—	0.5	—	0.5	—
Fraction inner-sphere MS	0.3	0.97	0.41	0.84	0.5	1	0.5	0.998	0.5	1	0.5	1
θ_{M}	0.014	0.018	0.02	0.026	0.026	0.03	0.026	0.036	0.026	0.033	0.026	0.035
$\bar{f}_{\text{B,M}}$ in V_{D}	50	950	5000	7700	50	930	5000	7700	50	940	5000	7800
$\log \bar{K}_{\text{int}}$ ($\text{m}^3 \text{ mol}^{-1}$) ^a	−0.52	−2.0	−1.8	−2.2	3.2	−0.1	2	−0.3	3	1.0	1.3	0.7

^a The \bar{K}_{int} for CCD is given by eqn (8) and for NICA-Donnan by eqn (7).



models show that the total concentration of intraparticulate Cd(II) is significantly reduced in the presence of excess Ca²⁺ (Tables 3 and 4). The CCD approach generates similar values for both θ_{Cd} and the intraparticulate concentration of free Cd²⁺

($=\bar{f}_{\text{B,M}}c_{\text{M,f}}^*$) in the two electrolytes, and consequently similar magnitudes of \bar{K}_{int} . The total concentration of intraparticulate Cd(II) in Ca(NO₃)₂ is lower than in KNO₃ by a factor of *ca.* 1/3, which reflects the absence of the condensed fraction (comprising 70% of the total intraparticulate Cd(II) in KNO₃; Table 3). Furthermore, we note that the \bar{K}_{int} value is comparable to the intrinsic affinity of simple carboxylate ligands, which is physicochemically reasonable for Cd(II) under these conditions, *e.g.* K_{int} (eqn (4)) for Cd-acetate is of the order 0.01 mol³ mol⁻¹.^{48,49} The NICA-Donnan derived \bar{K}_{int} values for Cd(II) are in broad agreement with the CCD result, being also of order 0.01 mol m⁻³ in both electrolytes. However, detailed examination reveals discrepancies in terms of the physicochemical reasonableness of the underlying parameters. Firstly, the concentration of intraparticulate free M²⁺ is a factor of *ca.* 10 higher in KNO₃ than in Ca(NO₃)₂. As a consequence, the θ_{Cd} in Ca(NO₃)₂ electrolyte is much lower, and the derived log \bar{K}_{int} value is *ca.* half a unit higher. In addition, the decrease in the total concentration of intraparticulate Cd(II) in Ca(NO₃)₂ is much greater than can be explained by electrostatic factors alone, *i.e.* the reduction in magnitude of the Donnan potential. These outcomes are a consequence of the NICA-Donnan assumption that Ca²⁺ association involves significant inner-sphere complexation, with consequent displacement of Cd²⁺ from its inner-sphere complexes with weaker sites.

For Cu(II), both the magnitude and the heterogeneity of the intrinsic chemical affinity of its complexes with HA are greater than those for Cd(II). Again, some notable differences in consistency of the interpretation by the CCD and NICA-Donnan models are apparent. At $I = 10 \text{ mol m}^{-3}$, the CCD approach shows that both θ_{Cu} and the intraparticulate concentration of free Cu²⁺ are significantly higher in Ca(NO₃)₂ electrolyte than in KNO₃. The total concentration of intraparticulate Cu(II) is approximately the same in both electrolytes, whilst the speciation changes from approximately equal amounts of condensed ions and inner-sphere complexes in KNO₃ (Table 3) to practically only inner-sphere complexes in Ca(NO₃)₂ (Table 4). The \bar{K}_{int} is *ca.* an order of magnitude lower in Ca(NO₃)₂ than in KNO₃ which predominantly reflects the *ca.* one order of magnitude higher θ_{Cu} . This result reflects the heterogeneity of the HA complexant: a greater proportion of intraparticulate inner-sphere complexes concomitantly means that the average affinity of the complexes is lower. NICA-Donnan derived results for Cu(II) at $I = 10 \text{ mol m}^{-3}$ show that the total concentration of intraparticulate Cu(II) and θ_{Cu} are the same in both electrolytes, and almost all of the particle-associated Cu(II) is predicted to be in the form of inner-sphere complexes in both cases. However, the intraparticulate concentration of free Cu²⁺ is a factor of *ca.* 3 lower in Ca(NO₃)₂. The lower concentration of free Cu²⁺ within the particle body has the consequence that the \bar{K}_{int} values obtained in Ca(NO₃)₂ are greater than those in KNO₃ (by *ca.* half a log unit). Others have reported that the presence of Ca²⁺ reduces

Table 4 Comparison of intraparticulate speciation obtained via the CCD and NICA-Donnan (NICAD) models for Ca(NO₃)₂ electrolyte. $c_{\text{M,I}}^* = 4.6 \times 10^{-3} \text{ mol m}^{-3}$; $c_{\text{HA,I}}^* = 50 \text{ g m}^{-3}$; pH = 6 in bulk electrolyte medium

	$\text{Cd}, I = 100 \text{ mol m}^{-3}$		$\text{Cd}, I = 10 \text{ mol m}^{-3}$		$\text{Pb}, I = 100 \text{ mol m}^{-3}$		$\text{Pb}, I = 10 \text{ mol m}^{-3}$		$\text{Cu}, I = 100 \text{ mol m}^{-3}$		$\text{Cu}, I = 10 \text{ mol m}^{-3}$	
	CCD	NICAD	CCD	NICAD	CCD	NICAD	CCD	NICAD	CCD	NICAD	CCD	NICAD
$c_{\text{M,I}}^*, \text{ mol m}^{-3}$	3.2×10^{-3}	3.8×10^{-3}	1.1×10^{-3}	3.4×10^{-3}	7.7×10^{-4}	5.2×10^{-4}	1.5×10^{-5}	1.9×10^{-4}	1.2×10^{-3}	6.1×10^{-5}	1.2×10^{-3}	3.5×10^{-4}
$c_{\text{M,I}}^*, \text{ mol m}^{-3}$	11	11	28	8.4	30	82	36	30	27	96	34	31
Fraction free in V_{DL}	1×10^{-4}	—	6×10^{-5}	—	9×10^{-6}	—	6×10^{-7}	—	2×10^{-5}	—	2×10^{-5}	—
Fraction free in V_{D}	3×10^{-3}	0.014	4×10^{-3}	0.06	3×10^{-4}	2×10^{-4}	4×10^{-5}	9×10^{-4}	5×10^{-4}	3×10^{-5}	1×10^{-3}	8×10^{-5}
Fraction inner-sphere MS	0.997	0.99	0.996	0.94	1	1	1	1	1	1	1	1
θ_{M}	0.016	0.004	0.04	0.009	0.043	0.033	0.052	0.034	0.039	0.038	0.048	0.035
$\bar{f}_{\text{B,M}}$ in V_{D}	11	40	105	140	11	40	105	140	11	40	105	140
$\log \bar{K}_{\text{int}} (\text{mol}^{-1})^a$	-0.35	-1.6	-0.46	-1.7	0.73	0.2	1.5	0.2	0.48	1.2	0.15	1.2

^a The \bar{K}_{int} for CCD is given by eqn (8) and for NICA-Donnan by eqn (7).



the extent to which Cd(II) is bound by HA, but has negligible impact on the extent of Cu(II)–HA complex formation.^{50,51} In the context of the NICA-Donnan model the inconsistent observation was explained by saying that Ca²⁺ hardly impacts on Cu–HA binding because the inner-sphere complexes of Cu(II) with phenolic type sites are stronger than those of Ca(II), whilst in the case of Cd(II), Ca²⁺ can compete for inner-sphere complexation of carboxyl groups.⁵⁰

5 Conclusions and outlook

Over the years a number of models have been developed to describe metal ion binding by HA. Each approach has provided insights into the nature of the association of ions with this charged, chemically heterogeneous complexant. Recent advances in understanding the physicochemical properties of soft, charged nanoparticles cast new light on M–HA complexation phenomena. In accounting for the electrostatic features of soft charged NPs such as HA, a purely Donnan type approach is demonstrated to be a physically incomplete description. Notably, Donnan partitioning by itself greatly underestimates the extent to which Ca²⁺ associates with HA, and even though covalency is essentially absent in Ca²⁺ binding, conventional equilibrium speciation models resort to inclusion of chemical affinity parameters to describe the Ca²⁺–HA association. Taking the NICA-Donnan approach as an example, there are several factors in the model that are out of line with experimental observations.^{34,35} These include *e.g.* the values of the protonation constants, the delineation and the ionic strength dependence of the Donnan volume, as well the magnitude of the Donnan potential. Each of the disparities acts to increase the extent of association of oppositely charged ions with the HA entity, thus pointing to possibly missing electrostatic ingredients in the interpretation. It is evident that the Ca²⁺–HA association involves stronger electrostatic interactions such as counterion condensation, potentially including the possibility for partial formation of inner-sphere ion pairs in which Ca_{aq}²⁺ exchanges some of its inner-sphere water of hydration.^{52,53} The CCD approach is shown to provide a more satisfactory physicochemical description of the electrostatic contribution to association of M²⁺ with HA.

There are significant differences in the intraparticle speciation predicted by the CCD and NICA-Donnan approaches. Notably, in 1–1 electrolyte the CCD approach finds a substantial electrostatic contribution to the association of Cd(II), Pb(II), and Cu(II) with HA. It follows that at the level of the \bar{K}_{int} values, the CCD and Donnan-only electrostatic models give significantly different results. For the heterogeneous HA complexant, \bar{K}_{int} is expected to increase as θ_{M} decreases. The CCD model retrieves this relationship, whilst the trend in the NICA-Donnan derived values is less systematic. Such differences in intraparticle speciation are highly significant for *e.g.* predictions of the lability and bioavailability of the complex species. For example, the present work has shown that for Pb–HA the total concentration of intraparticle Pb(II) is similar in KNO₃ and Ca(NO₃)₂ electrolyte, yet the lability of the complexes is very different in these two media, as a consequence of effect of the electrostatic environment in the NP body on the reaction rate constants.⁵⁴

A detailed exploration of the consequences of condensation phenomena on the intraparticle dynamics of M–HA complexes is underway.

Symbols and abbreviations

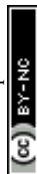
CC	Counterion condensation
D	Donnan phase
DL	Double layer
HA	Humic acid
<i>I</i>	Ionic strength
S	Reactive site
NP	Nanoparticle
SSCP	Stripping chronopotentiometry at scanned deposition potential
$c_{\text{M},f}^*$	Concentration of free metal ion in bulk electrolyte medium (mol m ⁻³)
$c_{\text{M},t}^*$	Total concentration of metal in the entire dispersion (mol m ⁻³)
$c_{\text{M},f}^{\text{DL}}$	Local concentration of free metal ion in the intraparticle double layer (mol m ⁻³)
$c_{\text{M},f}^{\text{D}}$	Local concentration of free metal ion in the Donnan volume (mol m ⁻³)
$c_{\text{M},\text{cond}}^{\text{DL}}$	Local concentration of condensed metal ion in the intraparticle double layer (mol m ⁻³)
$c_{\text{HA},t}^*$	Total smeared-out concentration of HA in the aqueous dispersion (g m ⁻³)
$c_{\text{M},f}$	Local average concentration of free metal ion in the particle body ($\varphi_{\text{DL}}c_{\text{M},f}^{\text{DL}} + \varphi_{\text{D}}c_{\text{M},f}^{\text{D}}$) (mol m ⁻³)
$c_{\text{M},t}$	Local total concentration of all forms of M in the particle body (mol m ⁻³)
c_{MS}	Local concentration of inner-sphere complex within the particle volume (mol m ⁻³)
c_{MS}^*	Smeared-out concentration of inner-sphere bound M (mol m ⁻³)
$c_{\text{S},t}^*$	Smeared-out total concentration of reactive sites (mol m ⁻³)
c_{S}^*	Smeared-out concentration of reactive sites (mol m ⁻³)
$c_{\text{S},t}$	Local total concentration of reactive sites within the particle volume (mol m ⁻³)
c_{S}	Local concentration of reactive sites within the particle volume (mol m ⁻³)
<i>e</i>	Elementary charge
$\bar{f}_{\text{B},\text{M}}$	Donnan partitioning factor for the metal ion
\bar{f}_{C}	Condensation factor in the intraparticle double layer
f^{os}	Concentration enhancement factor for M ²⁺ in the outer-sphere volume of an individual ion-pair in simple ligand case
<i>K</i>	Conventional stability constant for a simple ligand (m ³ mol ⁻¹)
K^{os}	Outer-sphere ion pair stability constant (m ³ mol ⁻¹)
\bar{K}_{app}	Apparent average stability constant for MHA based on smeared-out concentrations (m ³ mol ⁻¹)
\bar{K}_{int}	Intrinsic average stability constant for inner-sphere MS (m ³ mol ⁻¹)



κ^{-1}	Debye length in the bulk aqueous medium (m)
κ_{P}^{-1}	Intraparticulate Debye length (m)
ℓ_{DL}	Thickness of the intraparticulate condensation zone (m)
ℓ_{C}	Separation distance between charged sites (m)
n_{S}	Number of reactive sites per particle
r_{P}	Particle radius (m)
V_{D}	Volume of the Donnan phase (m^3)
V_{DL}	Volume of the intraparticulate double layer zone (m^3)
V^{os}	Outer-sphere volume for an ion pair between $\text{M}_{\text{aq}}^{2+}$ and an individual site S (m^3)
V_{P}	Volume of the NP entity (m^3)
ψ_{D}	Donnan potential (V)
ψ_{DL}	Potential at a given spatial position within the intraparticulate double layer (V)
$\bar{\rho}_{\text{DL}}$	Average volume charge density in the double layer ($\text{mol } e \text{ m}^{-3}$)
ρ_{P}	Structural volume charge density in the particle body ($\text{mol } e \text{ m}^{-3}$)
φ_{DL}	Particle volume fraction of the double layer zone
φ_{D}	Particle volume fraction of the Donnan zone
θ_{M}	Ratio of concentrations of inner-sphere complexes and reactive sites

References

- J. Buffle, *Complexation Reactions in Aquatic Systems: An Analytical Approach*, Ellis Horwood, Chichester, UK, 1988.
- L. K. Koopal, T. Saito, J. P. Pinheiro and W. H. van Riemsdijk, *Colloids Surf., A*, 2005, **265**, 40–54.
- E. Tipping, *Aquat. Geochem.*, 1998, **4**, 3–48.
- J. F. L. Duval, K. J. Wilkinson, H. P. van Leeuwen and J. Buffle, *Environ. Sci. Technol.*, 2005, **39**, 6435–6445.
- H. P. van Leeuwen and J. Buffle, *Environ. Sci. Technol.*, 2009, **43**, 7175–7183.
- R. M. Town, J. F. L. Duval, J. Buffle and H. P. van Leeuwen, *J. Phys. Chem. A*, 2012, **116**, 6489–6496.
- P. Warwick, A. Hall, S. J. King, J. Zhu and J. van der Lee, *Radiochim. Acta*, 1998, **81**, 215–221.
- A. P. Robertson and J. O. Leckie, *Environ. Sci. Technol.*, 1999, **33**, 786–795.
- R. Marsac, M. Davranche, G. Gruau, M. Bouhnik-Le Coz and A. Dia, *Geochim. Cosmochim. Acta*, 2011, **75**, 5625–5637.
- A. C. Montenegro, S. Orsetti and F. V. Molina, *Environ. Chem.*, 2014, **11**, 318–332.
- N. D. Bryan, D. M. Jones, M. Appleton, F. R. Livens, M. N. Jones, P. Warwick, S. King and A. Hall, *Phys. Chem. Chem. Phys.*, 2000, **2**, 1291–1300.
- M. F. Benedetti, W. H. van Riemsdijk and L. K. Koopal, *Environ. Sci. Technol.*, 1996, **30**, 1805–1813.
- I. Christl, A. Metzger, I. Heidmann and R. Kretzschmar, *Environ. Sci. Technol.*, 2005, **39**, 5319–5326.
- A. Liu and R. D. Gonzalez, *Langmuir*, 2000, **16**, 3902–3909.
- H. P. van Leeuwen and R. M. Town, *Environ. Chem.*, 2016, **13**, 76–83.
- G. S. Manning, *Biophys. Chem.*, 1977, **7**, 95–102.
- G. S. Manning, *Q. Rev. Biophys.*, 1978, **2**, 179–246.
- E. Garcia-Fernandez, P. M. R. Paulo and S. M. B. Costa, *Phys. Chem. Chem. Phys.*, 2015, **17**, 4319–4327.
- M. Majtyka and J. Kłos, *Phys. Chem. Chem. Phys.*, 2007, **9**, 2284–2292.
- Q. R. Huang, P. L. Dubin, C. N. Moorefield and G. R. Newkome, *J. Phys. Chem. B*, 2000, **104**, 898–904.
- Z. Li, A. K. van Dyk, S. J. Fitzwater, K. A. Fichthorn and S. T. Milner, *Langmuir*, 2016, **32**, 428–441.
- H. P. van Leeuwen, R. F. M. J. Cleven and P. Valenta, *Pure Appl. Chem.*, 1991, **63**, 1251–1268.
- R. M. Town and H. P. van Leeuwen, *Phys. Chem. Chem. Phys.*, 2016, **18**, 10049–10058.
- R. M. Fuoss, *J. Am. Chem. Soc.*, 1958, **80**, 5059–5061.
- H. P. van Leeuwen, R. M. Town and J. Buffle, *J. Phys. Chem. A*, 2007, **111**, 2115–2121.
- H. Ohshima and T. Kondo, *Biophys. Chem.*, 1990, **38**, 117–122.
- L. P. Yezek and H. P. van Leeuwen, *Langmuir*, 2005, **21**, 10342–10347.
- C. J. Milne, D. G. Kinniburgh, W. H. van Riemsdijk and E. Tipping, *Environ. Sci. Technol.*, 2003, **37**, 958–971.
- M. J. Avena, L. K. Koopal and W. H. van Riemsdijk, *J. Colloid Interface Sci.*, 1999, **217**, 37–48.
- W. F. Tan, L. K. Koopal and W. Norde, *Environ. Sci. Technol.*, 2009, **43**, 591–596.
- J. P. Pinheiro, A. M. Mota, J. M. R. d'Oliveira and J. M. G. Martinho, *Anal. Chim. Acta*, 1996, **329**, 15–24.
- M. Hosse and K. J. Wilkinson, *Environ. Sci. Technol.*, 2001, **35**, 4301–4306.
- J. F. L. Duval, *Langmuir*, 2005, **21**, 3247–3258.
- T. Lenoir, A. Matynia and A. Manceau, *Environ. Sci. Technol.*, 2010, **44**, 6221–6227.
- E. Companys, J. L. Garcés, J. Salvador, J. Galceran, J. Puy and F. Mas, *Colloids Surf., A*, 2007, **306**, 2–13.
- D. G. Kinniburgh, W. H. van Riemsdijk, L. K. Koopal, M. Borkovec, M. F. Benedetti and M. J. Avena, *Colloids Surf., A*, 1999, **151**, 147–166.
- J. F. L. Duval and H. P. van Leeuwen, *J. Phys. Chem. A*, 2012, **116**, 6443–6451.
- I. Christl, A. Metzger, I. Heidmann and R. Kretzschmar, *Environ. Sci. Technol.*, 2005, **39**, 5319–5326.
- L. Weng, E. J. M. Temminghoff, S. Lofts, E. Tipping and W. H. van Riemsdijk, *Environ. Sci. Technol.*, 2002, **36**, 4804–4810.
- K. Krishnan and R. A. Plane, *J. Am. Chem. Soc.*, 1968, **90**, 3195–3200.
- L. A. Clapp, C. J. Siddons, J. R. Whitehead, D. G. van Derveer, R. D. Rogers, S. T. Griffin, S. B. Jones and R. D. Hancock, *Inorg. Chem.*, 2005, **44**, 8495–8502.
- C. Travers and J. A. Marinsky, *J. Polym. Sci.*, 1974, **47**, 285–297.
- I. Christl, *Environ. Chem.*, 2012, **9**, 89–96.
- L. A. Oste, E. J. M. Temminghoff, T. M. Lexmond and W. H. van Riemsdijk, *Anal. Chem.*, 2002, **74**, 856–862.



- 45 J. Buffle, Z. Zhang and K. Startchev, *Environ. Sci. Technol.*, 2007, **41**, 7609–7620.
- 46 J. G. Hering and F. M. M. Morel, *Environ. Sci. Technol.*, 1988, **22**, 1234–1237.
- 47 W.-F. Tan, W. Norde and L. K. Koopal, *Geochim. Cosmochim. Acta*, 2011, **75**, 5749–5761.
- 48 A. Yuchi, H. Wada and G. Nakagawa, *Anal. Chim. Acta*, 1983, **149**, 209–216.
- 49 R. S. Kolat and J. E. Powell, *Inorg. Chem.*, 1962, **1**, 293–296.
- 50 D. G. Kinniburgh, C. J. Milne, M. F. Benedetti, J. P. Pinheiro, J. Filius, L. K. Koopal and W. H. van Riemsdijk, *Environ. Sci. Technol.*, 1996, **30**, 1687–1698.
- 51 J. Hamilton-Taylor, A. S. Postill, E. Tipping and M. P. Harper, *Geochim. Cosmochim. Acta*, 2002, **66**, 403–415.
- 52 F. J. Millero, F. Gombar and J. Oster, *J. Solution Chem.*, 1977, **6**, 269–280.
- 53 L. M. Hamm, A. F. Wallace and P. M. Dove, *J. Phys. Chem. B*, 2010, **114**, 10488–10495.
- 54 R. M. Town, *Environ. Chem.*, 2015, **12**, 130–137.

